Society of Medical Education & Research

2023, Volume 3, Issue 2, Page No: 75-95
ISSN: 3108-4826

Journal of Medical Sciences and Interdisciplinary Research

Tongguanteng Injection Inhibits Osteosarcoma Progression via the ER Stress-Linked IRE1/CHOP Pathway

Michal Tomasz Grabowski[1]*, Adrian Pawel Lis[1]

[1]Department of Management, Faculty of Economics, University of Wroclaw, Wroclaw, Poland.

***E-mail** ✉ m.grabowski.uwr@yahoo.com

Abstract

Tongguanteng injection (TGT) is widely utilized in China for treating or supporting therapy in multiple cancer types; however, its therapeutic efficacy and underlying mechanisms in osteosarcoma remain largely unexplored. Osteosarcoma cell lines 143B and MG-63 were exposed to varying concentrations of TGT. Cellular proliferation, migration, invasion, and apoptosis were assessed using CCK8 assays, transwell assays, and flow cytometry. Differentially expressed genes (DEGs) were identified via RNA sequencing (RNA-seq). The expression of key mRNAs and proteins linked to the IRE1/CHOP pathway was validated using RT-PCR and western blot analyses. To investigate the mechanism, the ER stress inhibitor 4-phenylbutyric acid (4-PBA) was employed. Additionally, 143B cells were transfected with siRNA to silence IRE1 or with the pEX-3-ERN1 plasmid to induce IRE1 overexpression. Downstream effectors, including CHOP and apoptosis-related proteins caspase-3 and PARP1, were examined. The in vivo anti-tumor effects of TGT were evaluated using a 143B xenograft mouse model, with tumor tissues subjected to H&E staining, TUNEL staining, and immunohistochemistry.

TGT markedly inhibited proliferation, migration, and invasion while promoting apoptosis in 143B and MG-63 osteosarcoma cells in vitro. Key DEGs included HSPA5 (encoding BiP), ERN1 (encoding IRE1), and DDIT3 (encoding CHOP), with "IRE1-mediated unfolded protein response" emerging as the most significantly enriched GO biological process. TGT treatment upregulated ER stress-associated proteins ATF6, BiP, p-IRE1, XBP1s, and CHOP, as well as cleaved caspase-3 and PARP1, suggesting induction of apoptosis via the IRE1/CHOP pathway. Inhibition of ER stress with 4-PBA or IRE1 knockdown attenuated TGT-induced expression of these proteins, whereas IRE1 overexpression enhanced CHOP levels and apoptosis. Consistently, in vivo administration of TGT suppressed tumor growth and increased p-IRE1 and CHOP expression in xenografted mice. significant anti-osteosarcoma activity both in vitro and in vivo, potentially through activation of the ER stress-related IRE1/CHOP pathway, highlighting this pathway as a promising therapeutic target in osteosarcoma.

Keywords: Tongguanteng injection, Osteosarcoma, Apoptosis, ER stress, IRE1/CHOP pathway

Introduction

Osteosarcoma is the most prevalent malignant bone tumor, predominantly affecting children and young adults aged 10–30 years [1]. Current treatments, primarily surgery combined with chemotherapy, have improved the 5-year survival rate to approximately 60% in patients with localized disease [2]; however, survival drops below 20% in cases of recurrent or metastatic osteosarcoma [1, 3]. Moreover, these treatments often result in long-term complications, including neurocognitive impairment, cardiomyopathy, and hepatic or renal toxicity, which may compromise patient outcomes [4]. Despite advancements over the past four decades, osteosarcoma management remains challenging due to limited effective pharmacological options, absence of specific therapeutic targets, and inconsistent responses to immunotherapy. Therefore, there is an urgent need to identify new anti-osteosarcoma agents that combine strong efficacy with low toxicity.

Access this article online https://smerpub.com/

Received: 01 May 2023; **Accepted:** 29 July 2023

How to cite this article: Grabowski MT, Lis AP. Tongguanteng Injection Inhibits Osteosarcoma Progression via the ER Stress-Linked IRE1/CHOP Pathway. J Med Sci Interdiscip Res. 2023;3(2):75-95. https://doi.org/10.51847/p1pOyJKAn3

Endoplasmic reticulum (ER) stress is frequently observed in tumor cells due to homeostatic imbalance triggered by diverse internal and external stimuli [5]. To restore ER equilibrium, cells activate three principal unfolded protein response (UPR) signaling branches: inositol-requiring enzyme 1α (IRE1α, or IRE1), protein kinase RNA-like ER kinase (PERK), and activating transcription factor 6 (ATF6), along with downstream transcription factors including X-box binding protein 1 (XBP1), ATF4, and C/EBP homologous protein (CHOP) [6]. When UPR fails to restore ER function, apoptosis is initiated. ER stress thus plays a dual role in tumor biology: while chronic ER stress can support cancer cell survival, deliberately inducing ER stress-mediated apoptosis has emerged as a potential anticancer strategy [7, 8]. Recent studies suggest that ER stress-targeting compounds, such as CYT997 (Lexibulin), may offer therapeutic potential against osteosarcoma [9–11]. The ER chaperone BiP (binding immunoglobulin protein), also known as GRP78 and encoded by HSPA5, is often overexpressed in cancers and serves as a primary ER stress sensor, directly interacting with UPR activators IRE1 and PERK to initiate the UPR [12–14].

The inositol-requiring enzyme 1 (IRE1), coded for by the ER to nucleus signaling 1 (ERN1) gene, serves as a key element in the unfolded protein response (UPR) pathway and possesses both protein kinase and endoribonuclease activities [15, 16].

When misfolded proteins accumulate in the endoplasmic reticulum, phosphorylated IRE1 (p-IRE1) performs unconventional splicing on XBP1 mRNA, producing the spliced variant known as XBP1s [17–19].

XBP1s then attaches to the promoter region of CHOP, enhancing its expression and ultimately resulting in cellular apoptosis [20, 21].

Moreover, IRE1 is capable of activating the downstream effector apoptotic-signaling kinase 1 (ASK1), which in turn stimulates Jun-N-terminal kinase (JNK) and p38 mitogen-activated protein kinase (p38 MAPK), thereby contributing to CHOP upregulation [20].

CHOP, encoded by DDIT3, acts as the primary mediator of apoptosis triggered by endoplasmic reticulum stress.

Recent investigations have revealed that curcumin modulates CHOP levels via ATF6, an additional important sensor in the ER stress response [22].

Additional research indicates that ATF6 modulates the UPR, an adaptive process mainly controlled by the dominant IRE1α and PERK branches [23].

Numerous reports have examined the induction of ER stress via IRE1 or CHOP to induce apoptosis in cancer cells [24–27].

Surfactin, a naturally occurring compound from Bacillus subtilis, induces apoptosis via the ER stress-related IRE1-ASK1-JNK signaling cascade in human osteosarcoma cells [9].

Coiled-coil domain containing 170 could stimulate the IRE1α-XBP1s axis to induce apoptosis in MCF7 breast cancer cells [28].

2-Bromopalmitate has been demonstrated to alter CHOP expression and enhance adriamycin-triggered apoptosis in osteosarcoma cells [29].

Tongguanteng injection (abbreviated as TGT), obtained from the traditional Chinese medicinal plant Marsdenia tenacissima (Roxb.) Wight et Arn., has been approved by the National Medical Products Administration (NMPA) for use in cancer treatment for more than two decades in China [30, 31].

To date, approximately 196 chemical constituents have been identified in the plant, among which C21 steroidal glycosides stand out as signature components responsible for anti-cancer activity through diverse pathways [30, 32].

TGT is frequently combined with chemotherapeutic agents for managing multiple malignancies, such as liver, gastric, and colon cancers.

Our earlier work demonstrated that TGT displays synergistic actions with chemotherapy and overcomes drug resistance in ovarian cancer [31, 33].

Research by T. Huang first showed that TGT can induce apoptosis in osteosarcoma cells, though with lower potency compared to doxorubicin [34].

In a recent publication from our group, network pharmacology combined with in vitro validation verified that TGT causes apoptosis in osteosarcoma cells in a dose-dependent fashion, with six C21 steroidal glycosides determined as the main active ingredients [35].

Nevertheless, the in vivo anti-osteosarcoma efficacy of TGT is still unknown, and its mechanistic basis requires additional investigation.

In this study, osteosarcoma cell lines along with a xenograft nude mouse model were established to assess the anti-tumor potential of TGT.

Moreover, to clarify the mechanistic details, the ER stress-linked IRE1/CHOP axis was examined through RNA-seq analysis.

Subsequent data revealed that TGT modulates the IRE1/CHOP signaling to induce apoptosis in osteosarcoma cells.

These results suggest that TGT represents a promising therapeutic option for osteosarcoma, but additional clinical confirmation via randomized controlled trials is required.

Materials and Methods

Drugs and reagents

TGT (batch No. 202108031) was supplied by Nanjing Sanhome Pharmaceutical Co., Ltd. (where 1 mL corresponds to 1 g of dried herbal powder).

The stems of M. tenacissima were sourced from Yunnan Province, China.

A voucher specimen (200907-T009-05) is deposited in the herbarium of Sanhome Pharmaceutical Co. Ltd. and was identified by Professor De-Kang Wu of Nanjing University of Chinese Medicine.

4-PBA (Cat. No. HY-A0281) was obtained from MedChemExpress (MCE, New Jersey, USA).

Cisplatin (batch No. 1M0696B03) was provided by Qilu Pharmaceutical Co., Ltd. (Jinan, China).

Antibodies against ATF6 (Cat. No. A0202), p-IRE1 (Cat. No. AP0878), IRE1 (Cat. No. A17940), PARP1 (Cat. No. A0942), BCL-2 (Cat. No. A19693), BAX (Cat. No. A19684), β-Actin (Cat. No. AF0003), and β-Tubulin (Cat. No. A12289) were sourced from ABclonal Technology Co., Ltd. (Wuhan, China).

Antibodies for BiP (Cat. No. 3177S) and cleaved caspase-3 (Cat. No. 9662S) were acquired from Cell Signaling Technology, Inc. (Boston, USA).

The CHOP antibody (Cat. No. 15204-1-AP) was purchased from Proteintech Group, Inc. (Wuhan, China).

The XBP1 antibody (Cat. No. ab220783) was supplied by Abcam Plc. (Cambridge, UK).

Cell culture and sources

The human osteosarcoma cell lines 143B and MG-63 were sourced from the Cell Bank of the Chinese Academy of Sciences (Shanghai, China). Primary human bone marrow mesenchymal stem cells (BMSCs) were procured from Procell Life Science & Technology Co., Ltd. (Wuhan, China). All cells were routinely cultured in Dulbecco's Modified Eagle Medium (DMEM; HyClone, USA) supplemented with 10% fetal bovine serum (FBS; Thermo Fisher Scientific, USA) and 1% penicillin/streptomycin mixture (NCM Biotech., China). Incubation was performed at 37 °C in a 5% CO_2 humidified environment. Subculturing was carried out every 48 hours using a 1:3 passage ratio.

Cell viability assessment using CCK-8

Cells were inoculated into 96-well culture plates at a density of 8×10^3 cells per well and allowed to attach overnight. Following attachment, cells were exposed to a range of TGT concentrations (20, 40, 60, 80, 100, 120, or 140 $mg \cdot mL^{-1}$). A vehicle-treated group served as the negative control. After 24 hours of exposure, 10 µL of CCK-8 solution (Beyotime Biotech., China) was introduced into each well, followed by further incubation for 1.5 hours at 37 °C. Absorbance readings were taken at 450 nm on a microplate reader (BioTek, Winooski, USA).

Clonogenic survival assay

To evaluate long-term proliferative potential, osteosarcoma cells were placed in 6-well plates at 5×10^3 cells per well and left to adhere overnight. Cells were subsequently treated with TGT at concentrations of 40, 60, or 80 $mg \cdot mL^{-1}$, while an untreated group acted as control. Treatment medium was removed after 24 hours and replaced with standard growth medium. Cultures were maintained until visible colonies comprised at least 50 cells. Fixation was achieved with 4% paraformaldehyde (15 min), followed by staining with 0.1% crystal violet (30 min). Colony counts were performed using ImageJ analysis software. Plating efficiency was expressed as a percentage: (colonies counted / cells seeded) × 100%.

Evaluation of migration and invasion potential

Horizontal migration was measured via scratch-wound assay. Osteosarcoma cells were grown to near-confluence (3×10^5 cells per well) in 6-well plates. A linear wound was created using a sterile 10 µL pipette tip. Cells were then administered TGT (40, 60, or 80 $mg \cdot mL^{-1}$), with an untreated set as control. Microscopic images of the wound were captured at 0 and 24 hours post-wounding using an inverted microscope (Leica DMi8, Wetzlar, Germany). Wound width analysis and closure percentage were computed with ImageJ software. Vertical migration and invasiveness were investigated using Transwell inserts (8.0 µm pores; Corning Costar, USA) in 24-well formats [36]. Invasion experiments involved pre-coating the insert membrane with 60 µL Matrigel ($3 mg \cdot mL^{-1}$), whereas migration assays omitted

Matrigel. The upper compartment received 200 µL of serum-free suspension (1×10^5 cells/mL) with varying TGT doses, while the lower compartment contained 600 µL of complete medium with 10% FBS as chemoattractant. Following 24 hours, cells on the upper surface were wiped away; migrated or invaded cells on the underside were fixed (4% paraformaldehyde, 15 min) and stained (0.1% crystal violet, 30 min). Quantification was done via ImageJ, with triplicates performed for each condition.

Nuclear morphology assessment with hoechst 33342

Cells were seeded in 6-well plates (3×10^5 cells/well), allowed to reach ~80% confluence, and then exposed to TGT (40 or 80 mg·mL^{-1}) for 24 hours. Untreated cultures served as controls. Hoechst 33342 dye (20 µL) was applied for 15 minutes, after which excess dye was washed off. Fluorescent images capturing chromatin condensation and nuclear fragmentation were acquired using a fluorescence microscope.

Apoptosis detection by flow cytometry

Osteosarcoma cells were cultured in 6-well plates (3×10^5 cells/well) until ~80% confluent and treated with TGT (40 or 80 mg·mL^{-1}) for 24 hours, with untreated cells as controls. All cells—both supernatant-suspended and trypsin-detached adherent populations—were collected. Staining for apoptosis was conducted using the FITC Annexin V Apoptosis Detection Kit I (BD Biosciences, USA) per the manufacturer's guidelines. Flow cytometric analysis (BD Biosciences, CA, USA) was used to determine the proportion of apoptotic cells.

Transcriptome sequencing (RNA-seq)

Osteosarcoma 143B cells were treated with TGT at concentrations of 40 or 80 mg·mL^{-1} for 24 hours. Three independent biological replicates were prepared for each treatment group as well as for the untreated control group. Total RNA isolation was performed using the EZ-press RNA Purification Kit (EZBioscience, Roseville, USA) in accordance with the manufacturer's guidelines. RNA concentration and purity were assessed with a microplate reader. Transcriptome libraries were constructed employing the VAHTS Universal V5 RNA-seq Library Prep Kit (Vazyme Biotech., China), involving mRNA fragmentation, first-strand cDNA synthesis, 3' end adenylation, adaptor ligation, and PCR enrichment. Library integrity and insert size were evaluated on an Agilent 2100 Bioanalyzer (CA, USA). Sequencing and subsequent bioinformatics processing were outsourced to OE Biotech Co., Ltd. (Shanghai, China). Paired-end 150 bp reads were generated on an Illumina NovaSeq 6000 platform, yielding approximately 50 million raw reads per sample. Clean reads were aligned to the reference genome with HISAT2, and gene expression was quantified in FPKM units. Raw read counts per gene were derived using HTSeq-count. Principal component analysis (PCA) was conducted in R (version 3.2.0) to confirm reproducibility across biological replicates. Normalization, fold-change calculation, and differential expression testing (assuming a negative binomial distribution) were carried out with DESeq2. Differentially expressed genes (DEGs) were defined using thresholds of q-value < 0.05 and $|\log_2(\text{fold change})| > 1$. Hierarchical clustering of DEGs was performed in R (version 3.2.0).

To identify genes exhibiting dose-dependent alterations in response to TGT, Short Time-series Expression Miner (STEM) software was employed. Gene Ontology (GO) and Kyoto Encyclopedia of Genes and Genomes (KEGG) pathway enrichment analyses for these TGT-responsive genes were performed based on the hypergeometric distribution.

Quantitative real-time PCR (qRT-PCR)

Total RNA was converted to cDNA using the EZBioscience Color Reverse Transcription Kit (EZBioscience, Roseville, USA) on a thermal cycler (42 °C for 15 min, followed by enzyme inactivation at 95 °C for 30 s). Quantitative PCR reactions were set up in 384-well plates with 2× Color SYBR Green qPCR Master Mix (ROX2 plus) (EZBioscience, Roseville, USA) according to the provided protocol. Amplification conditions consisted of an initial denaturation at 95 °C for 5 min, followed by 40 cycles of 95 °C for 10 s and 60 °C for 30 s. Expression levels were normalized to the housekeeping gene GAPDH. All primers **(Table 1)** were custom-synthesized by Sangon Biotech (Shanghai, China). Relative gene expression was calculated using the $2^{-\Delta\Delta Ct}$ method after determining mean Ct values. Each qRT-PCR experiment included three biological replicates and three technical replicates.

Table 1. Primer sequences for selected differentially expressed genes validated by quantitative PCR

Gene	Sequence (5′ → 3′)	Direction
MMP3	AGTCTTCCAATCCTACTG TTGCT	Forward

	TCCCCGTCACCTCCAATCC	Reverse
RHOJ	CTGATGAGCTACGCCAACGA	Forward
	GTCACAGTAACTGCATAGTGGTC	Reverse
KLHL4	GTGAGAAACGCGCACAAGATT	Forward
	AACCAACCTATGGGCTGGGAT	Reverse
KCNK10	GTGGTGGTCTACCTTGTCACT	Forward
	GGGCTCACACAGACATGATCC	Reverse
HSPA5	CATCACGCCGTCCTATGTCG	Forward
	CGTCAAAGACCGTGTTCTCG	Reverse
TIMP3	CATGTGCAGTACATCCATACGG	Forward
	CATCATAGACGCGACCTGTCA	Reverse
ERN1	CACAGTGACGCTTCCTGAAAC	Forward
	GCCATCATTAGGATCTGGGAGA	Reverse
DDIT3	GGAAACAGAGTGGTCATTCCC	Forward
	CTGCTTGAGCCGTTCATTCTC	Reverse

IRE1 knockdown using siRNAs and IRE1 overexpression (IRE1-OE) plasmid transfection

The sequences of human IRE1-specific small interfering RNAs (siRNAs), synthesized by GenePharma Co., Ltd. (Shanghai, China), are provided in **Table 2**. The human ERN1 gene (GenBank Accession: NM_001433.5) was amplified and subcloned into the pEX-3 (pGCMV/MCS/EGFP/NEO) vector to generate the IRE1 overexpression plasmid designated pEX-3-ERN1.

For transfection experiments, 143B cells were plated in 6-well plates at a density of 3×10^5 cells per well in antibiotic-free, reduced-serum medium (Gibco, USA). Transfections were performed using Lipofectamine™ 3000 reagent (Thermo Fisher Scientific, USA) according to the manufacturer's instructions.

For IRE1 knockdown, the transfection mixture consisted of 5 µL Lipofectamine™ 3000 Reagent and 100 nM IRE1 siRNA. Untransfected cells served as the blank control, while cells transfected with a non-targeting scrambled siRNA (siNC) were used as the negative control.

For IRE1 overexpression, the transfection complex included 5 µL Lipofectamine™ 3000, 5 µL P3000™ Reagent, and 2.5 µg of the IRE1-OE plasmid. Cells receiving the empty vector served as the control group.

Six hours post-transfection, the medium was replaced with fresh complete DMEM (HyClone, USA), and cells were incubated for an additional 48 hours. Protein lysates were then prepared, and transfection efficiency was assessed by Western blotting.

In the case of IRE1-OE plasmid transfection, stably expressing cells were selected using 200 µg/mL G-418 disulfate (MCE, USA) prior to protein extraction and Western blot analysis.

Table 2. Sequences of siRNAs targeting human IRE1

siRNA	Sequence (5′ → 3′)	Strand
siIRE1-1	CAGACAGACCUGCGUAAAUUC	Sense
	GAAUUUACGCAGGUCUGUCUG	Antisense
siIRE1-2	AUGGAGCUGAGGGCACAAUUG	Sense
	CAAUUGUGCCCUCAGCUCCAU	Antisense
siIRE1-3	GCCUGACGAAACUUCCUUUUA	Sense
	UAAAAGGAAGUUUCGUCAGGC	Antisense

Western blot analysis

Cells (143B) were lysed on ice for 30 minutes using RIPA lysis buffer supplemented with protease and phosphatase inhibitors (Beyotime Biotech., China; 100 µL per well in 6-well plates). Lysates were collected into Eppendorf tubes and clarified by centrifugation at 12,000 rpm for 20 minutes at 4 °C. Supernatants containing total protein were quantified using a BCA Protein Assay Kit (Beyotime Biotech., China). Sample protein levels were normalized to 1 µg/µL, with 15 µg loaded per lane. Proteins were mixed with loading buffer (ABclonal Biotech., China), denatured at 95 °C for 10 minutes, and resolved by SDS-PAGE before transfer to PVDF membranes. Membranes were blocked for 15 minutes using a rapid blocking solution (NCM Biotech., China) and probed overnight at 4 °C with primary antibodies (1:1000 dilution). The primary antibodies used were IRE1, p-IRE1, ATF6, PARP1, and β-Tubulin (ABclonal

Technology Co., Ltd., Wuhan, China); BiP and cleaved caspase-3 (Cell Signaling Technology, Inc., Boston, USA); CHOP (Proteintech Group, Inc., Wuhan, China); and XBP1 (Abcam Plc., Cambridge, UK). β-Tubulin served as the loading control. Following washes, membranes were incubated with HRP-conjugated secondary antibodies (1:5000) for 1 hour at room temperature. Signal detection was performed using ECL reagent (NCM Biotech., China), and band intensities were quantified with ImageJ software.

Establishment of xenograft tumor model

Male BALB/c nude mice (5–6 weeks old) were obtained from Shanghai Laboratory Animal Center (SLAC, Shanghai, China). Animals were housed in a specific pathogen-free facility with a 12-hour light/dark cycle, temperature maintained at 20–26 °C, and humidity at 40–70%. Food and water were provided ad libitum, with cage bedding changed every three days. All procedures were approved by the Animal Welfare Ethics Committee of Shanghai Sixth People's Hospital (Approval No. SYXK 2018-0028) and conducted in strict accordance with Chinese regulations on experimental animal use.

143B cells were harvested, washed three times in PBS, and resuspended at 1×10^6 cells per 100 µL. Cell suspensions were injected subcutaneously into the axillary region of each mouse. When tumor volumes reached 100–300 mm^3, animals were randomly assigned to five groups (n=8 per group): control (normal saline), cisplatin (3 $mg \cdot kg^{-1}$), low-dose TGT (10 $g \cdot kg^{-1}$), medium-dose TGT (20 $g \cdot kg^{-1}$), and high-dose TGT (40 $g \cdot kg^{-1}$). Cisplatin was delivered intraperitoneally every three days, whereas other treatments were administered daily by injection. Tumor dimensions were recorded daily using calipers, and volumes calculated as (length × $width^2$)/2. Treatment continued for 14 days, after which mice were anesthetized with 3% halothane and euthanized by cervical dislocation. Tumors were excised, photographed, weighed, and either snap-frozen in liquid nitrogen or fixed in 4% paraformaldehyde.

Hematoxylin and eosin (H&E) staining, TUNEL assay, and immunohistochemistry (IHC)

H&E staining was used to examine tissue morphology. Paraffin-embedded tumor samples were cut into 4 µm sections and mounted on slides. Following deparaffinization in xylene and rehydration through graded ethanol, sections from tumors as well as liver, heart, kidney, and lung tissues were stained with hematoxylin and eosin. Slides were then dehydrated, cleared in xylene, and mounted with coverslips. Microscopic images were captured using an Olympus microscope (Olympus Corporation, Tokyo, Japan).

Apoptotic DNA fragmentation was detected by TUNEL assay. Deparaffinized and rehydrated sections were treated with 3% H_2O_2 to block endogenous peroxidase activity. Staining was performed using the In Situ Cell Death Detection Kit, POD (Roche, Penzberg, Germany) according to the manufacturer's protocol, with signal amplification via DAB substrate (Beyotime Biotech., China).

Immunohistochemical staining was carried out to evaluate protein expression of p-IRE1, CHOP, and cleaved caspase-3. Antigen retrieval was achieved by boiling sections in sodium citrate buffer for 20 minutes. Non-specific binding was blocked with 5% BSA for 30 minutes. Primary antibodies against cleaved caspase-3, p-IRE1, and CHOP were applied overnight at 4 °C. After PBS washes, sections were incubated with secondary antibodies for 1 hour, followed by color development with DAB solution (Beyotime Biotech., China).

Statistical analysis

Data processing and visualization were performed using GraphPad Prism 8.0. Results are presented as mean ± standard deviation (SD). Intergroup differences were assessed by one-way analysis of variance (ANOVA) with Bonferroni post-hoc correction. A p-value < 0.05 was considered statistically significant.

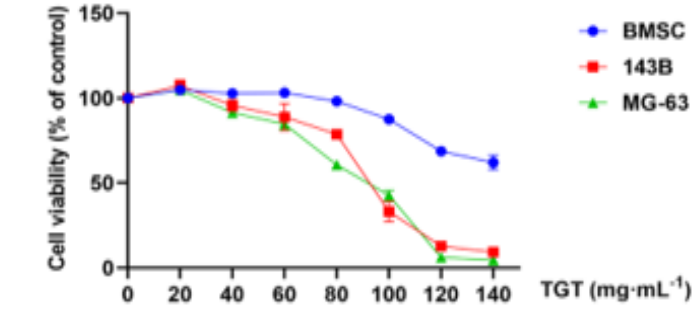

IC_{50} of TGT (mg·mL^{-1})	
143B	92.53±9.2
MG-63	87.44±0.54

a)

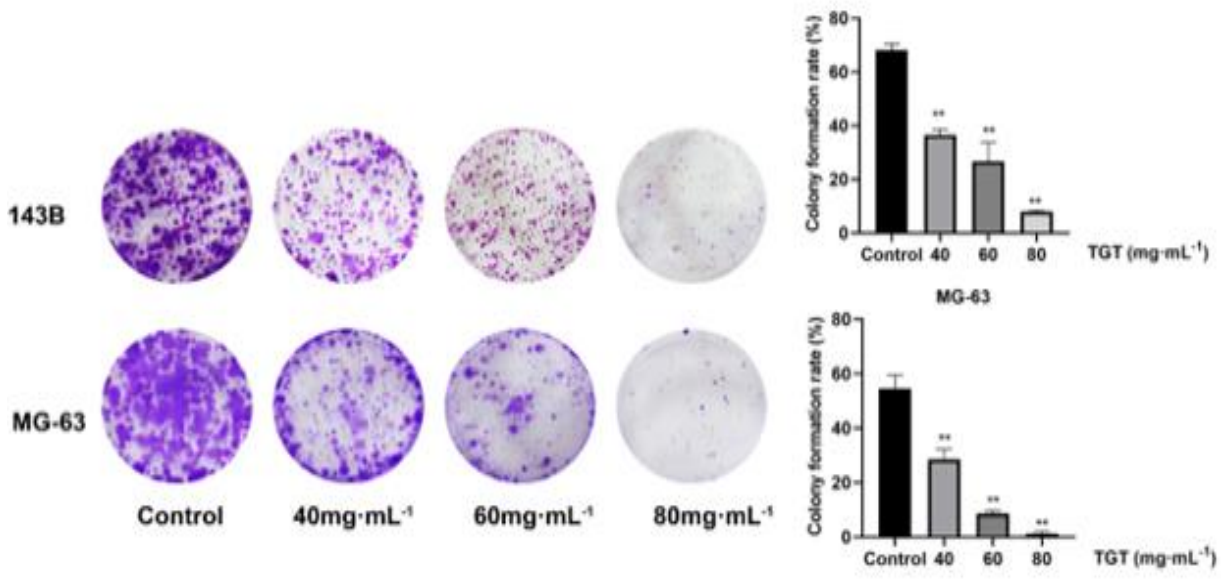

b)

Figure 1. TGT suppresses osteosarcoma cell proliferation. (a) 143B, MG-63, and BMSC cells were exposed to varying concentrations of TGT for 24 hours. Cell viability was assessed, and IC_{50} values were determined. (b) Following 24-hour exposure to TGT (40, 60, or 80 mg·mL^{-1}), the clonogenic capacity of 143B and MG-63 cells was evaluated. Values are presented as mean ± SD (n = 3). **p < 0.01 compared with the control group.

TGT restrains migration and invasion in osteosarcoma cells

Scratch-wound healing assays demonstrated a substantial decrease in horizontal migration ability in TGT-treated groups relative to controls **(Figure 2a)**. Additionally, Transwell experiments showed a marked reduction in both migrating and invading cell numbers in the TGT-exposed groups **(Figures 2b and 2c)**. Collectively, these findings confirm that TGT potently impedes the migratory and invasive properties of osteosarcoma cells.

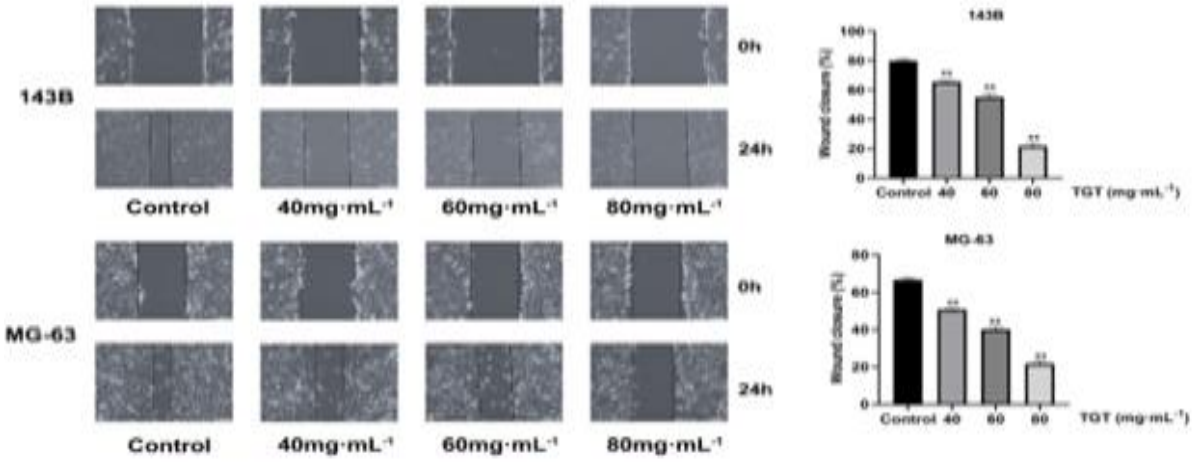

a)

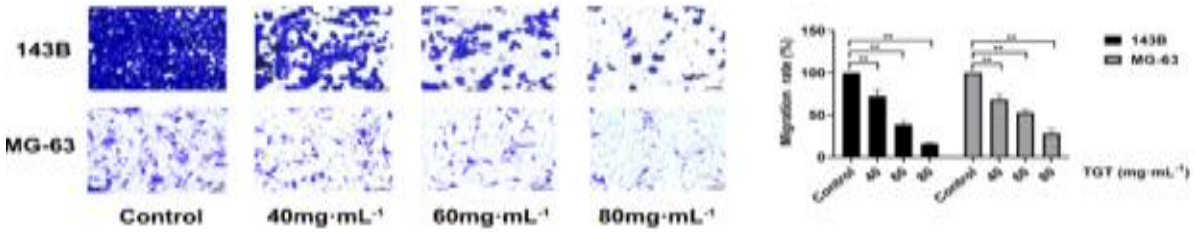

b)

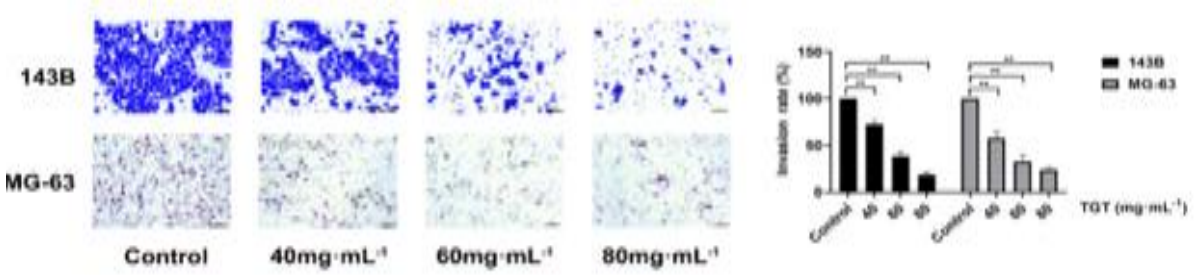

c)

Figure 2. TGT restricts the migratory and invasive potential of osteosarcoma cells. (a) TGT reduced horizontal migration of 143B and MG-63 cells as assessed by wound-healing scratch assay. Scale bar = 100 μm. (b) TGT diminished vertical migration of osteosarcoma cells in the Transwell migration assay. Scale bar = 50 μm. (c) TGT impaired the invasive capacity of osteosarcoma cells in the Matrigel-coated Transwell invasion assay. Scale bar = 50 μm. Results are shown as mean ± SD (n = 3). **p < 0.01 versus control group.

TGT promotes apoptosis in osteosarcoma cells

To investigate the pro-apoptotic effects of TGT on osteosarcoma cells (143B and MG-63), Hoechst 33342 staining was performed on cells treated with TGT for 24 hours. Compared to the control group, TGT-treated cells displayed characteristic apoptotic features, including decreased cell density and brightly condensed nuclei **(Figure 3a)**. These morphological alterations became more pronounced at higher TGT concentrations. In agreement with the staining observations, flow cytometry revealed a concentration-dependent increase in apoptotic rates following TGT exposure **(Figure 3b)**. Western blot analysis further corroborated these findings, showing upregulated BAX protein levels and downregulated BCL-2 expression in TGT-treated groups **(Figure 3c)**.

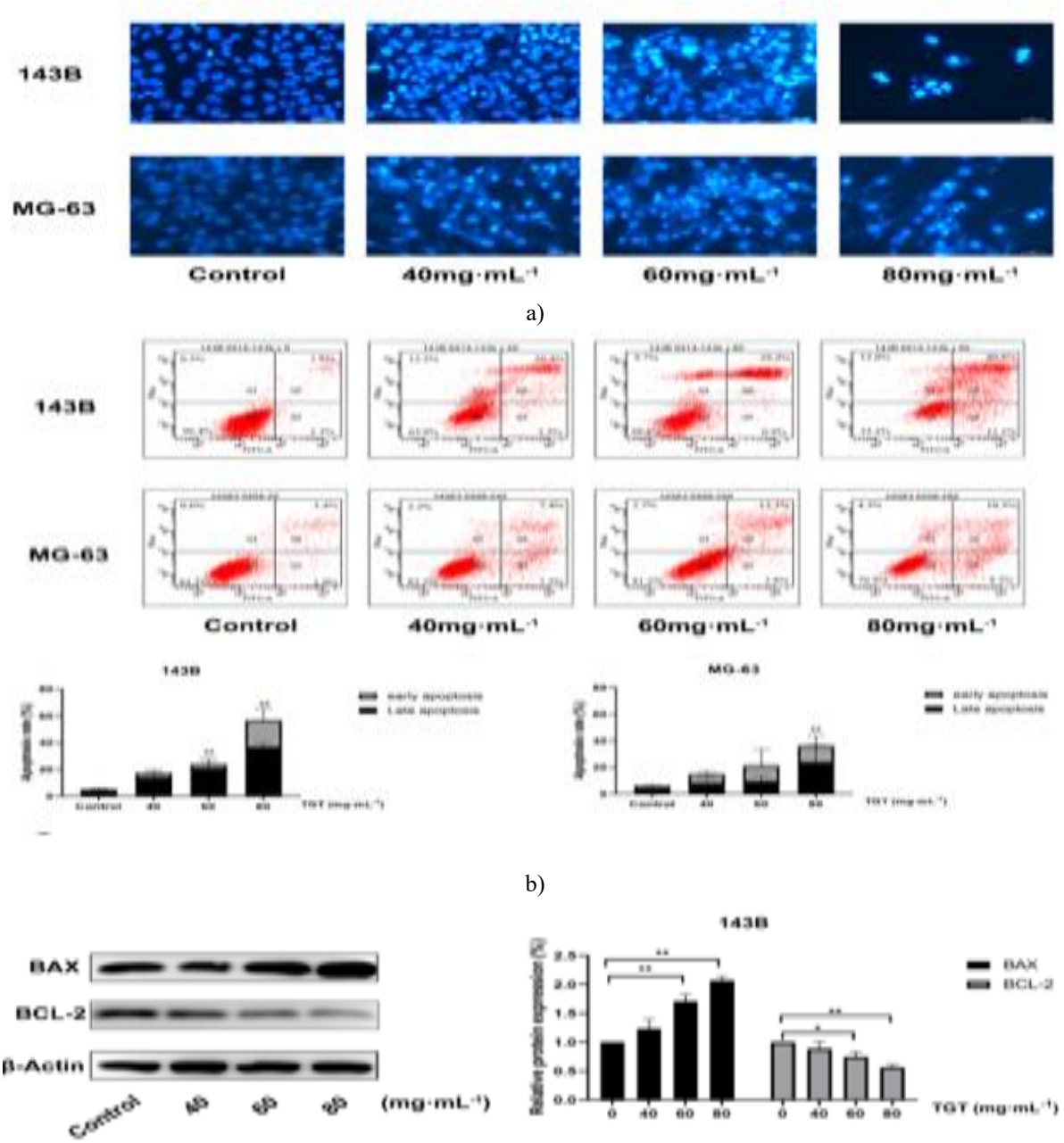

Figure 3. TGT induces apoptosis in osteosarcoma cells. (a) TGT triggered apoptotic changes in 143B and MG-63 cells as revealed by Hoechst staining. Scale bar = 25 μm. (b) TGT elevated the apoptotic fraction of osteosarcoma cells as measured by flow cytometry. (c) TGT administration upregulated BAX protein levels while downregulating BCL-2, as determined by Western blotting. Results are shown as mean ± SD (n = 3). *p < 0.05, **p < 0.01 compared to the control group.

RNA sequencing analysis of TGT-treated 143B cells

In this study, RNA-seq was performed on osteosarcoma 143B cells to identify genes modulated by TGT that contribute to apoptosis. Cells were treated with two doses of TGT (40 and 80 mg·mL^{-1}) and differentially expressed genes (DEGs) were determined by comparison to the untreated control. DEGs were filtered using criteria of q-value < 0.05 and $|\log_2 FC| > 1$. Relative to controls, 63 and 328 DEGs were detected in the low- and high-dose groups, respectively. Volcano plots highlighted that the

apoptosis-related gene DDIT3 exhibited one of the highest fold changes in both treatment conditions **(Figure 4a)**. Notably, ERN1 and HSPA5 showed strong upregulation in the 80 mg·mL^{-1} group **(Figure 4a)**.

To confirm the RNA-seq findings, eight randomly chosen DEGs (four upregulated and four downregulated) were subjected to qRT-PCR validation. Relative expression levels were computed using the $2^{-}\Delta\Delta Ct$ method, with statistical analysis via one-way ANOVA followed by Bonferroni correction. The qRT-PCR results aligned with the sequencing data for all genes except KLHL4 **(Figure 4b)**. Consistent with the volcano plot observations, the ER stress-related genes ERN1 and HSPA5 displayed marked overexpression **(Figure 4b)**.

Short Time-series Expression Miner (STEM) analysis identified 16 distinct expression profiles. Profiles 13, 12, and 15 showed trends positively associated with the ER stress response pathway. Gene Ontology (GO) enrichment for genes in profile 15 indicated that "IRE1-mediated unfolded protein response" was the top enriched biological process, while Kyoto Encyclopedia of Genes and Genomes (KEGG) analysis identified "Protein processing in endoplasmic reticulum" as the most significantly enriched pathway **(Figure 4c)**.

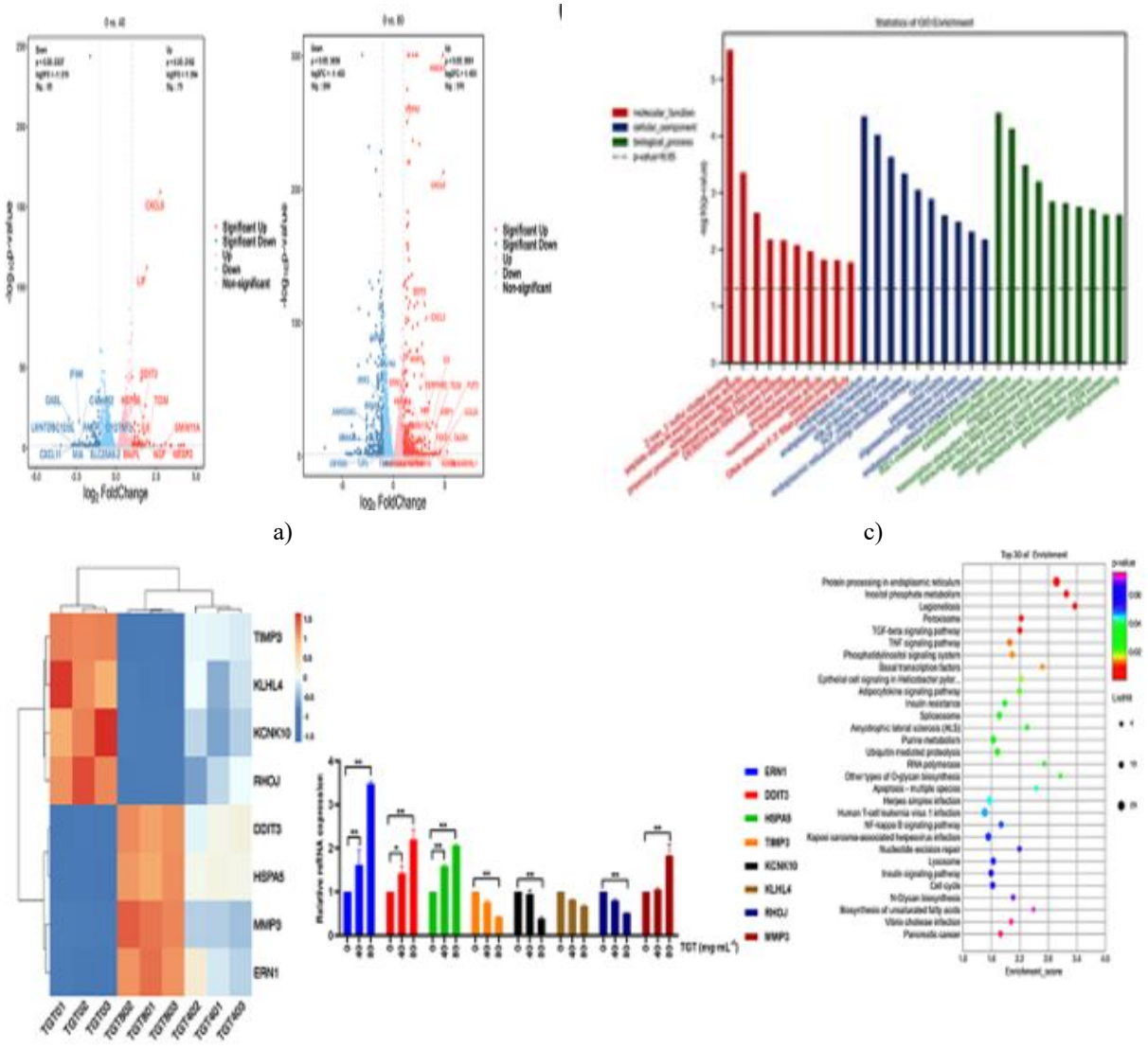

Figure 4. Transcriptome profiling of 143B cells following 24-hour TGT exposure. (a) Volcano plots displaying differentially expressed genes (DEGs) filtered by q-value < 0.05 and $|\log_2 FC| > 1$ in the 40 and 80 mg·mL^{-1} TGT treatment groups. (b) Heatmap illustration and qRT-PCR confirmation of ER stress-related genes along with

randomly chosen DEGs. (c) Gene Ontology (GO) and Kyoto Encyclopedia of Genes and Genomes (KEGG) enrichment analyses for genes assigned to profile 15. Values are presented as mean ± SD (n = 3). *p < 0.05, **p < 0.01 relative to the control group.

TGT stimulates the IRE1/CHOP axis and drives cellular apoptosis

To examine the connection between endoplasmic reticulum stress and TGT-triggered apoptosis in osteosarcoma cells, Western blotting was employed to assess protein levels of ATF6, BiP, IRE1, XBP1, and CHOP. TGT treatment markedly elevated the expression of ATF6, BiP, p-IRE1, XBP1s, and CHOP in 143B osteosarcoma cells **(Figure 5a)**, indicating activation of ER stress responses. Concurrently, TGT substantially increased the levels of cleaved caspase-3 and cleaved PARP1 in these cells **(Figure 5b)**. These observations suggest that TGT enhances IRE1 phosphorylation, thereby engaging the IRE1/CHOP signaling cascade, provoking ER stress, and ultimately promoting apoptosis in 143B osteosarcoma cells.

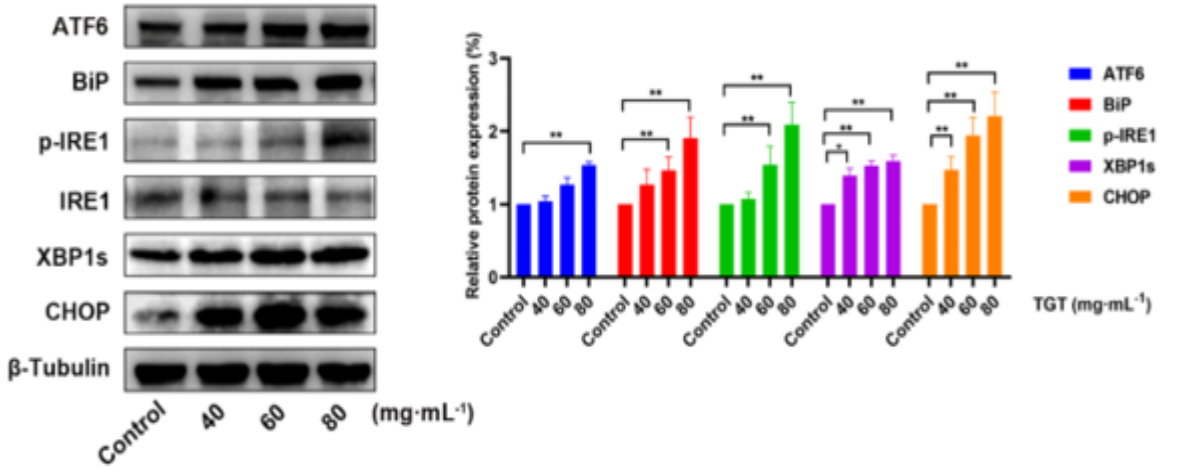

a)

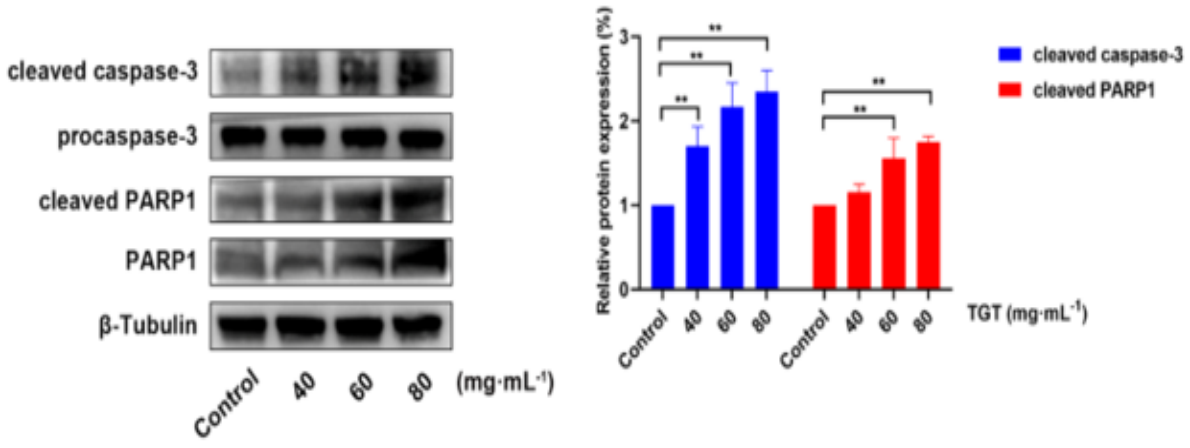

b)

Figure 5. TGT activates the endoplasmic reticulum stress pathway and apoptotic markers in 143B cells. (a) TGT exposure increased protein levels of ATF6, BiP, p-IRE1, XBP1s, and CHOP, as determined by Western blotting. (b) TGT treatment elevated the levels of cleaved caspase-3 and cleaved PARP1, as assessed by Western blotting. Results are presented as mean ± SD (n = 3). *p < 0.05, **p < 0.01 compared with the control group.

IRE1 silencing mitigates ER stress responses and apoptosis

To assess the involvement of IRE1 in TGT-mediated ER stress, specific siRNAs targeting IRE1 were synthesized and efficiently introduced into cells. Among them, siIRE1-3 exhibited the greatest knockdown efficacy and was chosen for subsequent experiments to disrupt the ER stress signaling in osteosarcoma cells **(Figure 6a)**. As demonstrated in **Figure 6b**, IRE1 depletion led to reduced protein expression of ATF6, BiP, p-IRE1, XBP1s, and CHOP relative to the TGT-alone group. In addition, levels of cleaved caspase-3 and cleaved PARP1 were markedly lowered, accompanied by a decrease in the apoptotic rate **(Figures 6c and 6d)**.

The established ER stress inhibitors 4-phenylbutyric acid (4-PBA) and tauroursodeoxycholic acid (TUDCA) are commonly employed across various disease models, including malignancies, and have demonstrated excellent safety in vivo [37–39]. Prior reports indicate that 4-PBA suppresses ER stress in osteosarcoma, whereas no such data exist for TUDCA to date [40, 41]. Administration of 4-PBA produced a modestly greater suppression of apoptosis-associated proteins and apoptotic rates compared to IRE1 knockdown **(Figures 6c and 6d)**. Collectively, these data support the conclusion that TGT induces ER stress-dependent apoptosis in 143B osteosarcoma cells primarily via the IRE1/CHOP axis.

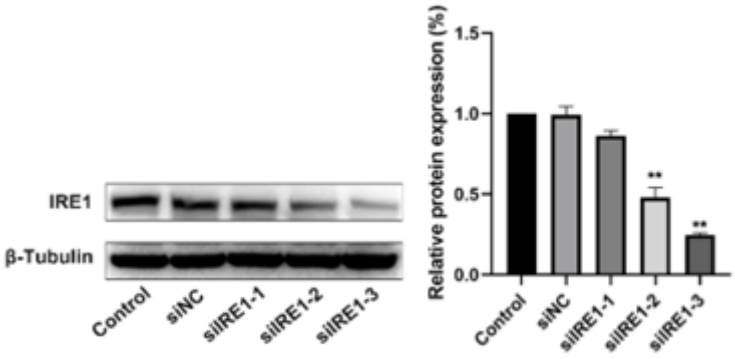

a)

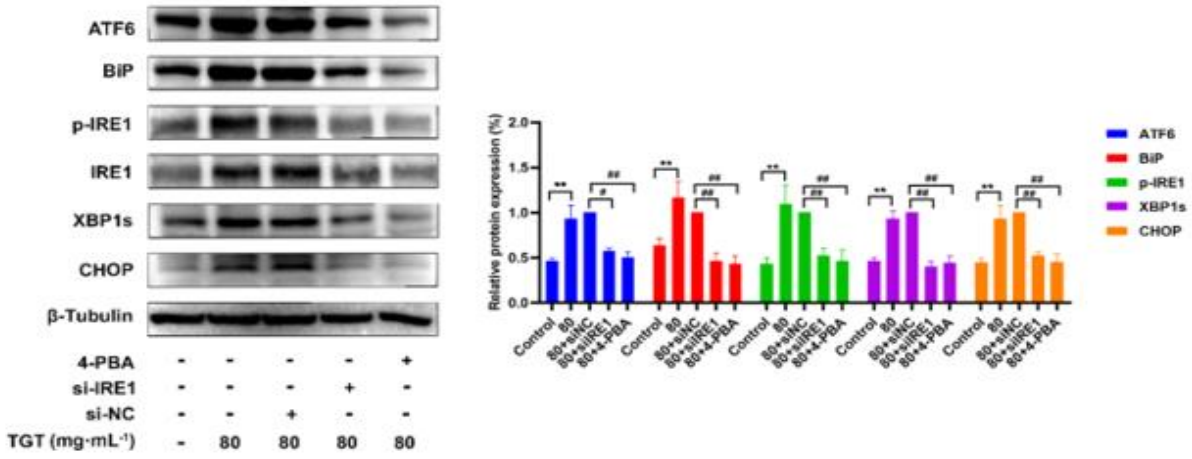

b)

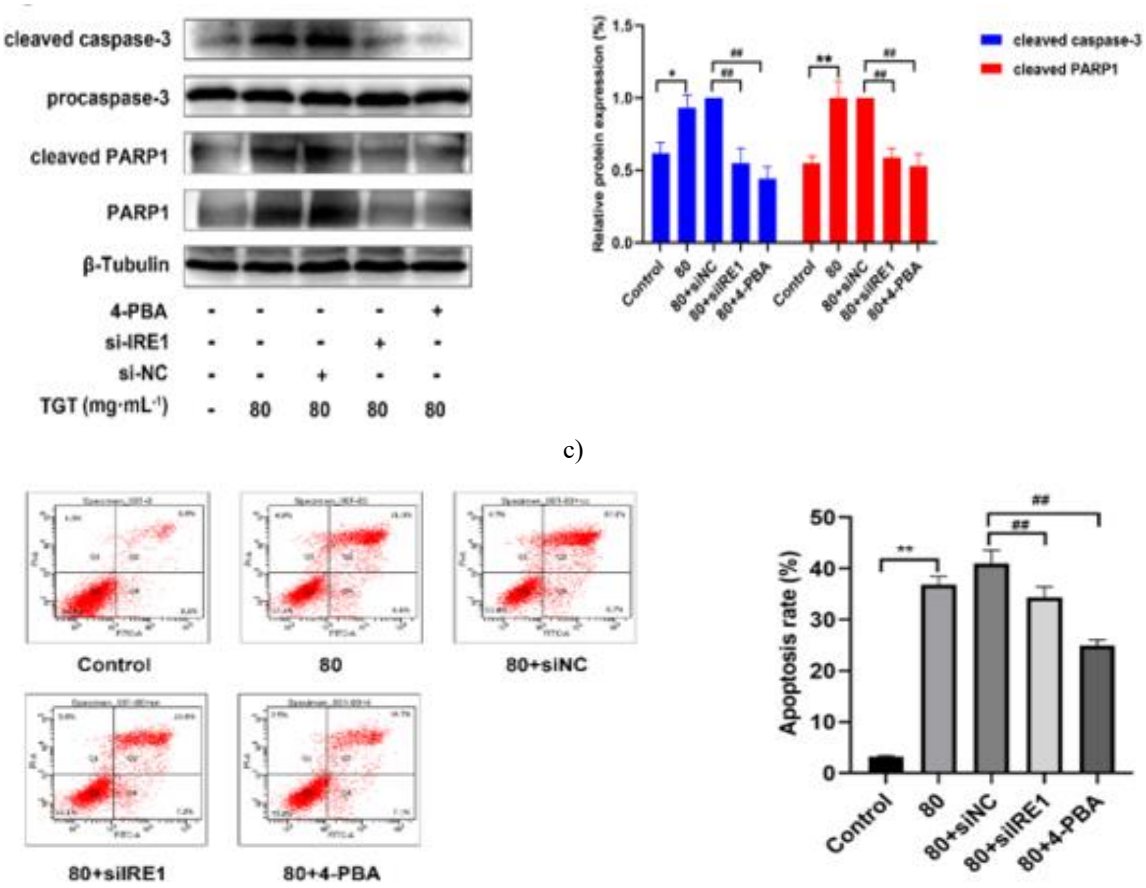

Figure 6. Silencing IRE1 or blocking ER stress reduces apoptosis in 143B cells. (a) Knockdown efficacy of three siRNAs targeting IRE1 was evaluated by Western blotting. (b) Protein levels of ER stress regulators, including ATF6, BiP, p-IRE1, XBP1s, and CHOP, were substantially lowered following IRE1 knockdown, as shown by Western blot analysis. (c) IRE1 depletion markedly decreased the levels of cleaved caspase-3 and cleaved PARP1, as assessed by Western blotting. (d) Both IRE1 knockdown and 4-PBA treatment significantly lowered the apoptotic rate, as measured by flow cytometry. Results are presented as mean ± SD (n = 3). #p < 0.05, ##p < 0.01 versus control group; *p < 0.05, **p < 0.01 versus TGT-only group.

IRE1 overexpression augments CHOP levels and promotes apoptosis in 143B cells

To further elucidate the link between the IRE1/CHOP axis and ER stress-mediated apoptosis in 143B cells, an IRE1 overexpression plasmid (IRE1-OE) was introduced into the cells. Overexpression of IRE1 led to a pronounced increase in CHOP protein expression. Additionally, the apoptosis execution markers cleaved caspase-3 and cleaved PARP1 exhibited elevated levels **(Figure 7a)**. Clonogenic assays revealed reduced colony-forming ability, while flow cytometry confirmed heightened apoptosis in IRE1-overexpressing cells **(Figures 7b and 7c)**. These findings demonstrate that elevated IRE1 expression boosts CHOP production and drives apoptotic cell death in 143B cells.

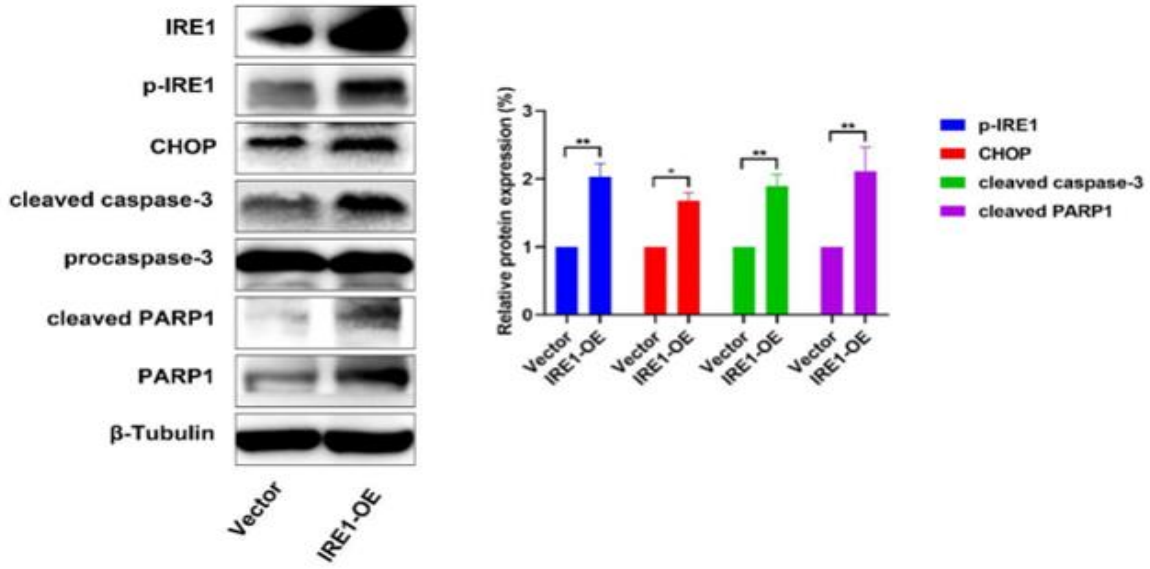

a)

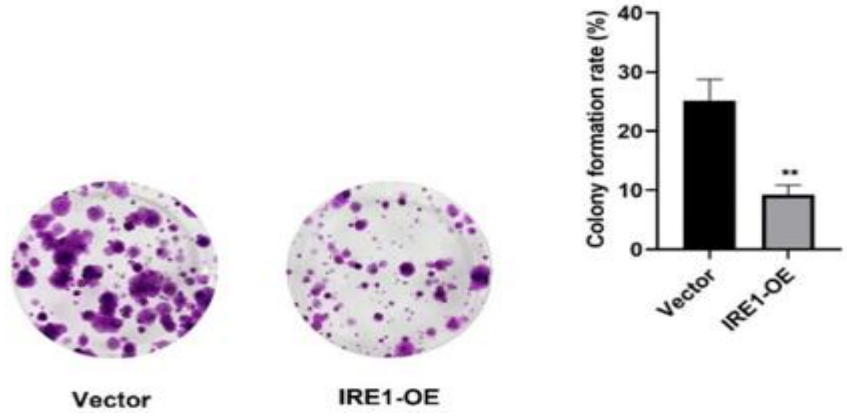

b)

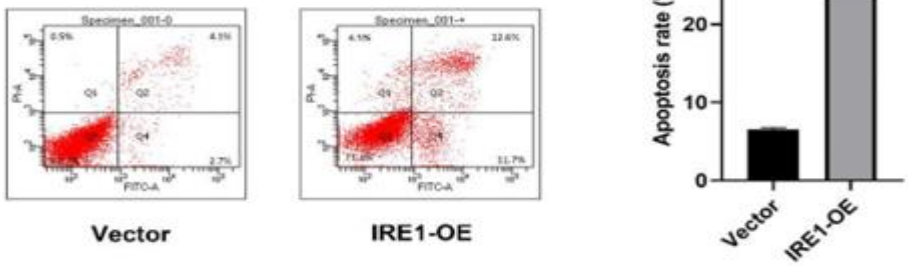

c)

Figure 7. IRE1 overexpression promotes CHOP expression and apoptosis in 143B cells. (a) Western blot analysis showed increased levels of IRE1, CHOP, cleaved caspase-3, and cleaved PARP1 in 143B cells transfected with the IRE1-OE plasmid. (b) The colony formation ability of 143B cells was reduced following IRE1 overexpression. (c) The apoptosis level of the 143B cells was reduced upon IRE1 overexpression, as determined by flow cytometry. Data are presented as mean ± SD (n = 3). *p < 0.05, **p < 0.01 vs. control.

TGT exerts anti-osteosarcoma effects via the IRE1/CHOP pathway in vivo

To assess the therapeutic potential of TGT against osteosarcoma, a nude mouse xenograft model was established, with cisplatin serving as a positive control. TGT treatment significantly reduced tumor volume and weight, though not to the extent observed with cisplatin. Importantly, mice receiving TGT maintained stable body weight, comparable to the control group, whereas cisplatin-treated mice experienced notable weight loss **(Figure 8a)**. H&E staining of major organs revealed no significant histological changes in the heart, liver, or lungs across low, medium, and high TGT doses, and no kidney damage was observed at the low dose, although occasional eosinophilic deposits appeared in renal tubules at medium and high doses. No tissue necrosis or inflammatory infiltration was detected in any organs following TGT treatment, whereas cisplatin caused mild organ toxicity, including myocardial necrosis, hepatocyte swelling, pulmonary granulocyte infiltration, and renal eosinophilic deposits **(Figure 8b)**. These findings indicate that TGT effectively suppresses osteosarcoma growth in vivo with minimal toxicity. Consistent with in vitro results, TUNEL staining confirmed that TGT increased tumor cell apoptosis, and immunohistochemistry showed upregulation of p-IRE1, CHOP, and cleaved caspase-3 following TGT treatment **(Figure 8c)**. Overall, these data demonstrate that TGT exerts anti-osteosarcoma effects in vivo, likely through activation of ER stress pathways.

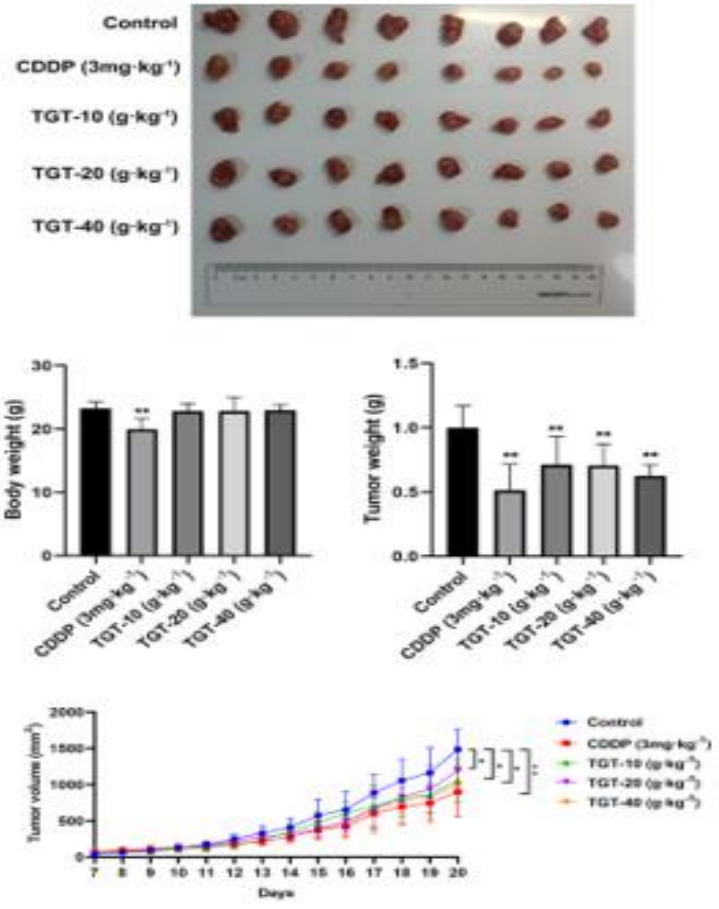

a)

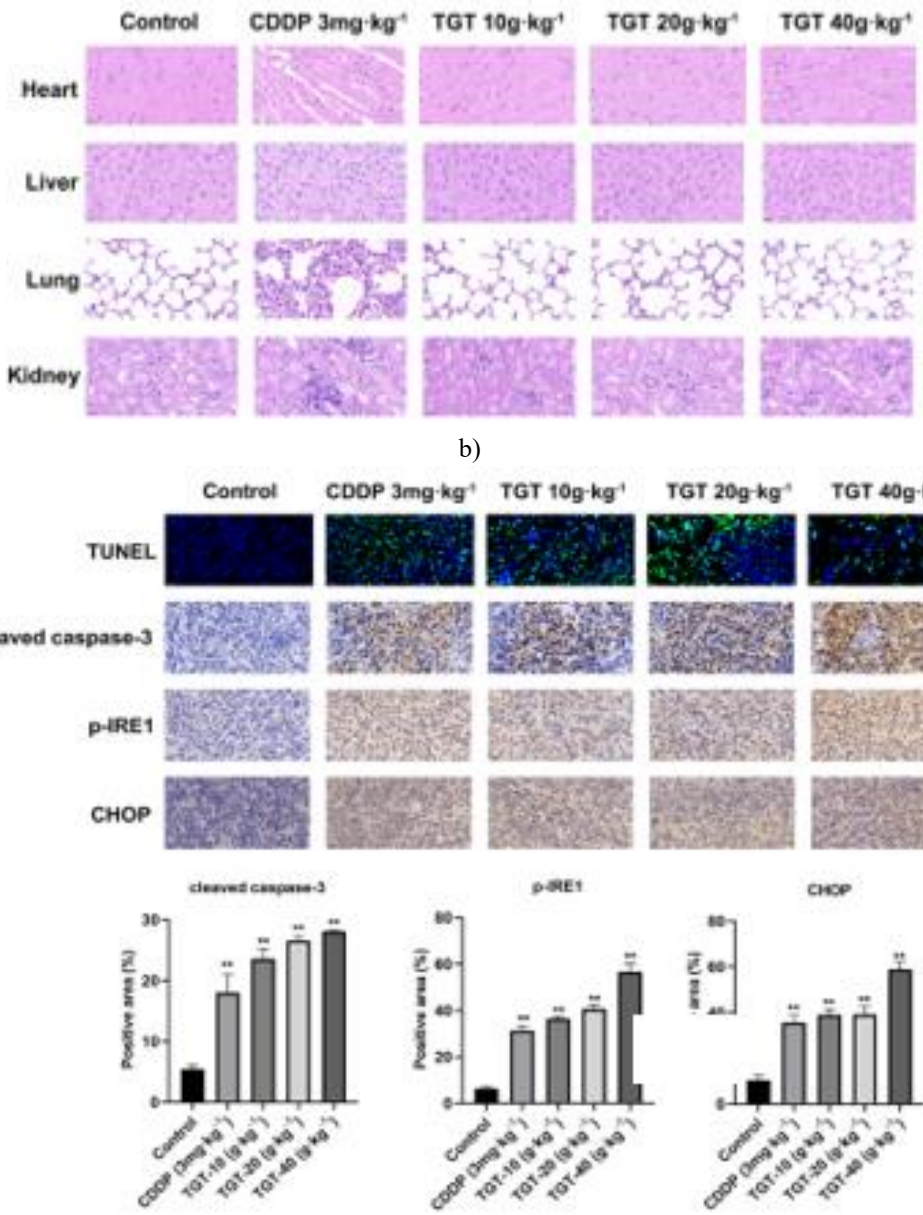

Figure 8. TGT suppresses osteosarcoma progression in vivo via the IRE1/CHOP pathway. (a) Tumor morphology, body weight, and tumor growth curves are presented (mean ± SD, n = 8). (b) Representative H&E-stained images of heart, liver, lung, and kidney tissues from mice in each group (400×, n = 3, Scale bar = 20 μm). (c) TGT-induced apoptosis in tumor cells (TUNEL staining, 400×) and increased levels of cleaved caspase-3, p-IRE1, and CHOP (IHC staining, 400×) in the xenograft model (mean ± SD, n = 3, Scale bar = 20 μm). *p < 0.05, **p < 0.01, compared with control.

Osteosarcoma represents the most prevalent primary malignant bone tumor, with surgery and chemotherapy as standard treatments, yielding overall survival rates of 60–75% [42, 43]. Nevertheless, therapeutic advancements over the past four decades have been minimal, highlighting the need for novel treatment strategies. TGT has demonstrated notable antitumor properties, suggesting its potential utility in clinical oncology. Prior studies reported that TGT induces dose-dependent apoptosis in osteosarcoma 143B and SAOS2 cells, aligning with our findings [34, 35]. However, the precise mechanisms of TGT in osteosarcoma remain unclear.

In this study, TGT inhibited proliferation, migration, and invasion of 143B and MG-63 osteosarcoma cells in vitro. RNA sequencing was employed to identify differentially expressed genes (DEGs) in 143B cells treated with TGT, leading to the identification of potential target genes, including DDIT3 and ERN1. The CHOP protein, encoded by DDIT3, is a key transcription factor in the ER stress response, typically expressed at very low levels under physiological conditions. ER stress, induced by pathological stimuli or microbial infection, increases CHOP expression and promotes apoptosis [20]. Overexpression of CHOP can also trigger osteosarcoma cell apoptosis through multiple signaling pathways [11, 29].

Our results revealed that TGT upregulated HSPA5 and ERN1 expression, confirmed by RT-PCR and further validated at the 40 mg·mL−1 concentration by q-PCR. Given the enrichment of the "IRE1-mediated unfolded protein response" biological process, it is plausible that TGT activates the IRE1/CHOP pathway to induce osteosarcoma cell apoptosis [44].

ER stress is increasingly recognized as having dual roles in cancer, supporting either cell survival or apoptosis [7, 11, 45, 46]. Three primary UPR signaling branches—IRE1-, PERK-, and ATF6-mediated pathways—are activated in response to ER stress. While the UPR initially aims to restore protein homeostasis, persistent stress can trigger apoptosis via CHOP upregulation, caspase-3 cleavage, and PARP1 inactivation [47, 48]. In IRE1-dependent ER stress, XBP1s plays a central role: initially induced by ATF6 and subsequently spliced by IRE1, XBP1s binds the CHOP promoter to enhance its expression, culminating in apoptosis [49].

Accordingly, we assessed the expression of ER stress-related proteins, including p-IRE1, ATF6, BiP, XBP1s, and CHOP, in 143B cells. TGT treatment significantly increased their levels, with IRE1 undergoing phosphorylation, a modification essential for its activation [50], indicating that TGT stimulates IRE1 activity and downstream ER stress signaling. Additionally, TGT elevated cleaved caspase-3 and cleaved PARP1 levels, confirming induction of apoptosis. Although ATF6 can fine-tune the UPR, the PERK pathway was unaffected by TGT in our study [21, 23, 51]. Literature supports that activating ER stress via IRE1 promotes tumor cell apoptosis [9]. Collectively, these findings suggest that TGT may facilitate dissociation of the IRE1-BiP complex, activating IRE1 and downstream transcription factors XBP1 and CHOP. IRE1 can either suppress or promote tumor development depending on the context [52–54]. To determine whether TGT induces apoptosis in osteosarcoma cells via ER stress through the IRE1/CHOP pathway, IRE1 expression was silenced using siRNA. Knockdown of IRE1 led to reduced levels of downstream transcription factors XBP1s and CHOP, as well as decreased ATF6 and BiP expression. BiP, a major ER chaperone, serves as a primary sensor for UPR activation; under normal conditions, it binds to ATF6, PERK, and IRE1 to maintain them in an inactive state. ER stress triggers BiP dissociation, enhancing its expression [55, 56]. Therefore, downregulation of IRE1 suppressed ER stress, leading to reduced BiP expression, while decreased ATF6 and XBP1s further attenuated ER stress. Additionally, TGT treatment combined with si-IRE1 significantly lowered cleaved caspase-3 and cleaved PARP1 levels and reduced apoptosis, which was corroborated by treatment with the ER stress inhibitor 4-PBA [44]. These findings indicate that IRE1 plays a central role in TGT-induced ER stress via the IRE1/CHOP pathway, regulating osteosarcoma cell apoptosis.

To further validate these results, IRE1 was overexpressed in 143B cells, which enhanced CHOP and apoptosis-associated proteins cleaved caspase-3 and cleaved PARP1. Caspase-3, a key executioner of apoptosis, is activated during ER stress either directly or indirectly and cleaves substrates like PARP1, leading to apoptotic execution [57, 58]. Consistent with prior studies showing CHOP-mediated activation of caspase-3 and PARP1, our data indicate that IRE1 overexpression upregulates CHOP and triggers apoptosis. Collectively, these findings demonstrate that TGT promotes osteosarcoma cell apoptosis through the ER stress-associated IRE1/CHOP pathway in vitro.

The anti-osteosarcoma effect of TGT was further confirmed in a xenograft tumor model. In vivo experiments showed that TGT activated apoptosis via the IRE1/CHOP pathway, accompanied by increased p-IRE1 and CHOP expression in tumor tissues. Interestingly, TUNEL staining revealed that a higher TGT dose (40 g·kg−1) resulted in a lower apoptosis rate than a 20 g·kg−1 dose, likely due to non-apoptotic cell death mechanisms such as autophagy, necrosis, or ferroptosis, which TUNEL cannot detect. Previous research from our

group demonstrated that TGT can induce autophagy in 143B cells, though autophagy was not the primary cause of cell death, supporting this explanation [36].

Growing evidence suggests that targeting ER stress is a promising cancer therapy strategy [59]. Many studies have attempted to modulate ER stress-associated proteins, including IRE1. Hyperactivating IRE1 to switch its role from pro-survival to pro-apoptotic may represent a potential antitumor approach [28, 60]. In line with this, our study showed that TGT induced IRE1 phosphorylation, promoting its activity and activating downstream ER stress signaling, ultimately leading to osteosarcoma cell apoptosis and antitumor effects. However, due to tumor-type and context-dependent variations, most therapeutic approaches targeting IRE1 have focused on inhibition rather than activation [25]. CHOP, a pro-apoptotic regulator, is crucial for inducing cancer cell apoptosis [26, 27]. In our study, CHOP was identified as a downstream target of IRE1 in osteosarcoma, and TGT effectively engaged the IRE1/CHOP pathway to exert anti-osteosarcoma effects. Nonetheless, further clinical validation is necessary to evaluate efficacy, specificity, and safety before translation into clinical therapy.

Conclusion

This study demonstrates that TGT exerts potent anti-osteosarcoma effects by activating the IRE1/CHOP pathway, thereby inducing apoptosis in osteosarcoma cells **(Figure 9)**. These findings provide new insights into TGT's antitumor mechanisms and suggest its potential as a therapeutic strategy for osteosarcoma. However, the specific bioactive components responsible for these effects remain unidentified, and further research is needed to clarify the precise roles of CHOP and other IRE1-regulated proteins in osteosarcoma and their influence on cell fate.

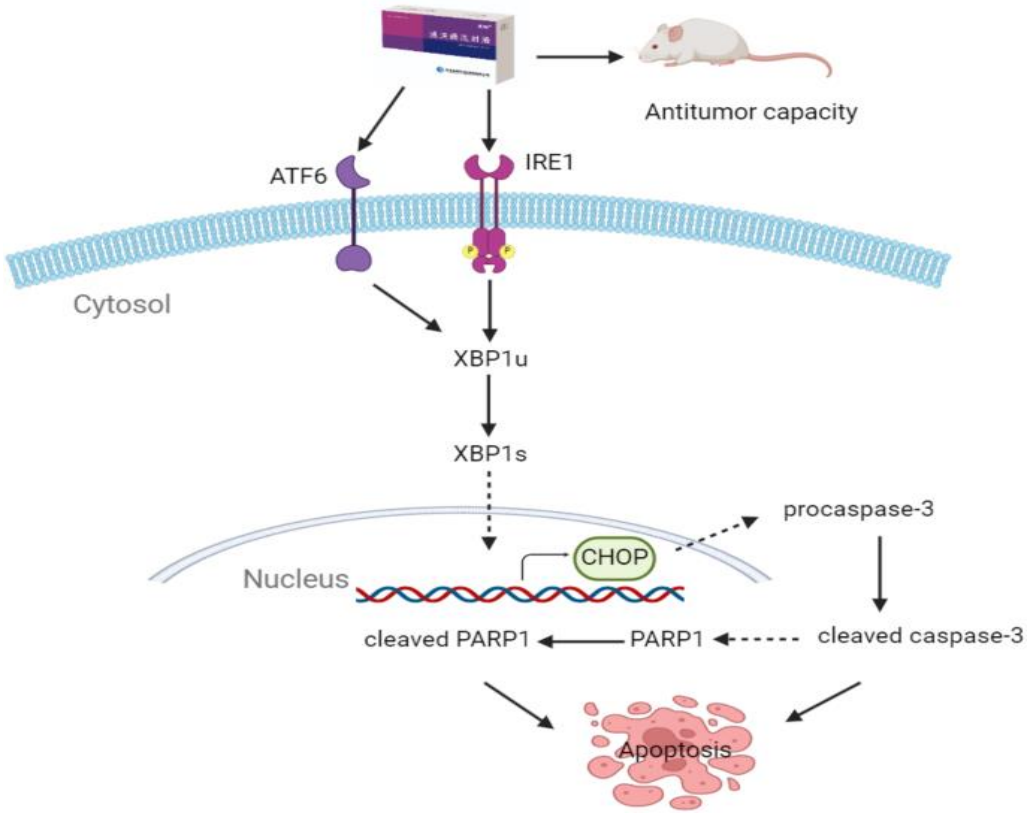

Figure 9. TGT inhibits the growth of osteosarcoma through the ER stress-associated IRE1/CHOP pathway

Acknowledgments: None

Conflict of Interest: None

Financial Support: None

Ethics Statement: None

References

1. Meltzer PS, Helman LJ. New horizons in the treatment of osteosarcoma. N Engl J Med. 2021;385(22):2066–76.
2. Beird HC, Bielack SS, Flanagan AM, et al. Osteosarcoma Nat Rev Dis Primers. 2022;8(1):77.
3. Shoaib Z, Fan TM, Irudayaraj JMK. Osteosarcoma mechanobiology and therapeutic targets. Br J Pharmacol. 2022;179(2):201–17.
4. Hudson MM, Bhatia S, Casillas J, et al. Long-term follow-up care for childhood, adolescent, and young adult cancer survivors. Pediatrics. 2021;148(3):e2021053127.
5. Chen X, Cubillos-Ruiz JR. Endoplasmic reticulum stress signals in the tumour and its microenvironment. Nat Rev Cancer. 2021;21(2):71–88.
6. Urra H, Dufey E, Avril T, et al. Endoplasmic reticulum stress and the hallmarks of Cancer. Trends Cancer. 2016;2(5):252–62.
7. Oakes SA. Endoplasmic reticulum stress signaling in cancer cells. Am J Pathol. 2020;190(5):934–46.
8. Salvagno C, Mandula JK, Rodriguez PC, et al. Decoding endoplasmic reticulum stress signals in cancer cells and antitumor immunity. Trends Cancer. 2022;8(11):930–43.
9. Wang GS, Chen JY, Chen WC, et al. Surfactin induces ER stress-mediated apoptosis via IRE1-ASK1-JNK signaling in human osteosarcoma. Environ Toxicol. 2022;37(3):574–84.
10. Wang Z, Yin F, Xu J, et al. CYT997 (Lexibulin) induces apoptosis and autophagy through the activation of mutually reinforced ER stress and ROS in osteosarcoma. J Exp Clin Cancer Res. 2019;38(1):44.
11. Zhao A, Zhang Z, Zhou Y, et al. β-Elemonic acid inhibits the growth of human osteosarcoma through endoplasmic reticulum (ER) stress-mediated PERK/eIF2α/ATF4/CHOP activation and Wnt/β-catenin signal suppression. Phytomedicine. 2020;69:153183.
12. Zhang T, Li J, Yang M, et al. CDK7/GRP78 signaling axis contributes to tumor growth and metastasis in osteosarcoma. Oncogene. 2022;41(40):4524–36.
13. Farshbaf M, Khosroushahi AY, Mojarad-Jabali S, et al. Cell surface GRP78: an emerging imaging marker and therapeutic target for cancer. J Control Release. 2020;328:932–41.
14. Kopp MC, Larburu N, Durairaj V, et al. UPR proteins IRE1 and PERK switch BiP from chaperone to ER stress sensor. Nat Struct Mol Biol. 2019;26(11):1053–62.
15. Madhavan A, Kok BP, Rius B, et al. Pharmacologic IRE1/XBP1s activation promotes systemic adaptive remodeling in obesity. Nat Commun. 2022;13(1):608.
16. Bashir S, Banday M, Qadri O, et al. The molecular mechanism and functional diversity of UPR signaling sensor IRE1. Life Sci. 2021;265:118740.
17. Grandjean JMD, Madhavan A, Cech L, et al. Pharmacologic IRE1/XBP1s activation confers targeted ER proteostasis reprogramming. Nat Chem Biol. 2020;16(10):1052–61.
18. Park SM, Kang TI, So JS. Roles of XBP1s in transcriptional regulation of target genes. Biomedicines. 2021;9(7):791.
19. Acosta-Alvear D, Karagöz GE, Fröhlich F, et al. The unfolded protein response and endoplasmic reticulum protein targeting machineries converge on the stress sensor IRE1. Elife. 2018;7:e43036.
20. Hu H, Tian M, Ding C, et al. The C/EBP homologous protein (CHOP) transcription factor functions in endoplasmic reticulum stress-induced apoptosis and microbial infection. Front Immunol. 2018;9:3083.
21. Yang Y, Liu L, Naik I, et al. Transcription factor C/EBP homologous protein in health and diseases. Front Immunol. 2017;8:1612.
22. Liang J, Chen J, Yang L, et al. Curcumin alleviates atrazine-induced cardiotoxicity by inhibiting endoplasmic reticulum stress-mediated apoptosis in mice through ATF6/Chop/Bcl-2 signaling pathway. Biomed Pharmacother. 2024;171:116205.
23. Cubillos-Ruiz JR, Bettigole SE, Glimcher LH. Tumorigenic and immunosuppressive effects of endoplasmic reticulum stress in cancer. Cell. 2017;168(4):692–706.
24. Jiang D, Niwa M, Koong AC. Targeting the IRE1α-XBP1 branch of the unfolded protein response in human diseases. Semin Cancer Biol. 2015;33:48–56.

25. Raymundo DP, Doultsinos D, Guillory X, et al. Pharmacological targeting of IRE1 in cancer. Trends Cancer. 2020;6(12):1018–30.
26. Yang IH, Jung JY, Kim SH, et al. ABT-263 exhibits apoptosis-inducing potential in oral cancer cells by targeting C/EBP-homologous protein. Cell Oncol (Dordr). 2019;42(3):357–68.
27. Kim H, Shin EA, Kim CG, et al. Obovatol induces apoptosis in non-small cell lung cancer cells via C/EBP homologous protein activation. Phytother Res. 2016;30(11):1841–7.
28. Wang Q, Zhao Y, Zheng H, et al. CCDC170 affects breast cancer apoptosis through IRE1 pathway. Aging. 2020;13(1):1332–56.
29. Xu T, Huang C, Qi XT, et al. 2-Bromopalmitate sensitizes osteosarcoma cells to adriamycin-induced apoptosis via the modulation of CHOP. Eur J Pharmacol. 2019;844:204–15.
30. Wang P, Yang J, Zhu Z, et al. Marsdenia tenacissima: a review of traditional uses, phytochemistry and pharmacology. Am J Chin Med. 2018;46 (07):1449–80.
31. Zhang XQ, Ding YW, Chen JJ, et al. Xiaoaiping injection enhances paclitaxel efficacy in ovarian cancer via pregnane X receptor and its downstream molecules. J Ethnopharmacol. 2020;261:113067.
32. Wang X, Yan Y, Chen X, et al. The antitumor activities of Marsdenia tenacissima. Front Oncol. 2018;8:473.
33. Kong QW, Yang J, Li D, et al. Tongguanteng injection reverses paclitaxel resistance via upregulation of table 1 expression in ovarian cancer in vitro and in vivo. J Ethnopharmacol. 2023;300:115728.
34. Huang T, Gong WH, Zou CP, et al. Marsdenia tenacissima extract sensitizes MG63 cells to doxorubicin-induced apoptosis. Genet Mol Res. 2014;13(1):354–62.
35. Wei L, Meng J, Xiang D, et al. Network pharmacology and experimental validation to study the potential mechanism of Tongguanteng injection in regulating apoptosis in osteosarcoma. BMC Complement Med Ther. 2024;24(1):67.
36. Justus CR, Marie MA, Sanderlin EJ, et al. Transwell in vitro cell migration and invasion assays. Methods Mol Biol. 2023;2644:349–59.
37. Xia SW, Wang ZM, Sun SM, et al. Endoplasmic reticulum stress and protein degradation in chronic liver disease. Pharmacol Res. 2020;161:105218.
38. Wang L, Hu T, Shen Z, et al. Inhibition of USP1 activates ER stress through Ubi-protein aggregation to induce autophagy and apoptosis in HCC. Cell Death Dis. 2022;13(11):951.
39. Lai KM, Wang JH, Lin SC, et al. Crassolide induces G2/M cell cycle arrest, apoptosis, and autophagy in human lung cancer cells via ROS-mediated ER stress pathways. Int J Mol Sci. 2022;23(10):5624.
40. Jiang J, Wang W, Xiang W, et al. The phosphoinositide 3-kinase inhibitor ZSTK474 increases the susceptibility of osteosarcoma cells to oncolytic vesicular stomatitis virus VSVΔ51 via aggravating endoplasmic reticulum stress. Bioengineered. 2021;12(2):11847–57.
41. Chiu KW, Chen HY, Chen CL, et al. Attenuation of endoplasmic reticulum stress enhances carvacrol-induced apoptosis in osteosarcoma cell lines. Life (Basel). 2023;13(3):744.
42. Angulo P, Kaushik G, Subramaniam D, et al. Natural compounds targeting major cell signaling pathways: a novel paradigm for osteosarcoma therapy. J Hematol Oncol. 2017;10(1):10.
43. Gill J, Gorlick R. Advancing therapy for osteosarcoma. Nat Rev Clin Oncol. 2021;18(10):609–24.
44. Xue W, Sun R, Hao Z, et al. Heterophyllin B ameliorates gastric cancer tumor growth through activating ER stress. Tissue Cell. 2023;83:102129.
45. Zhu P, Li T, Li Q, et al. Mechanism and role of endoplasmic reticulum stress in osteosarcoma. Biomolecules. 2022;12(12):1882.
46. Siwecka N, Rozpędek W, Pytel D, et al. Dual role of endoplasmic reticulum stress-mediated unfolded protein response signaling pathway in carcinogenesis. Int J Mol Sci. 2019;20(18):4354.
47. Jiang M, Qi L, Li L, et al. The caspase-3/GSDME signal pathway as a switch between apoptosis and pyroptosis in cancer. Cell Death Discov. 2020;6:112.
48. Xu H, Shen X, Li X, et al. The natural product dehydrocurvularin induces apoptosis of gastric cancer cells by activating PARP-1 and caspase-3. Apoptosis. 2023;28:525–38.
49. Yoshida H, Matsui T, Yamamoto A, et al. XBP1 mRNA is induced by ATF6 and spliced by IRE1 in

response to ER stress to produce a highly active transcription factor. Cell. 2001;107(7):881–91.
50. Belyy V, Zuazo-Gaztelu I, Alamban A, et al. Endoplasmic reticulum stress activates human IRE1α through reversible assembly of inactive dimers into small oligomers. Elife. 2022;11:e74342.
51. Han J, Back SH, Hur J, et al. ER-stress-induced transcriptional regulation increases protein synthesis leading to cell death. Nat Cell Biol. 2013;15(5):481–90.
52. Zheng J, Guo Y, Shi C, et al. Differential Ire1 determines loser cell fate in tumor-suppressive cell competition. Cell Rep. 2023;42(11):113303.
53. Martinez-Turtos A, Paul R, Grima-Reyes M, et al. IRE1α overexpression in malignant cells limits tumor progression by inducing an anti-cancer immune response. Oncoimmunology. 2022;11(1):2116844.
54. Yang S, Jiang H, Bian W, et al. Bip-Yorkie interaction determines oncogenic and tumor-suppressive roles of Ire1/Xbp1s activation. Proc Natl Acad Sci U S A. 2022;119(42):e2202133119.
55. Brahim IM, Abdelmalek DH, Elfiky AA. GRP78: a cell's response to stress. Life Sci. 2019;226:156–63.
56. Xia S, Duan W, Liu W, et al. GRP78 in lung cancer. J Transl Med. 2021;19(1):118.
57. Hsu HY, Lin TY, Hu CH, et al. Fucoidan upregulates TLR4/CHOP-mediated caspase-3 and PARP activation to enhance cisplatin-induced cytotoxicity in human lung cancer cells. Cancer Lett. 2018;432:112–20.
58. Meng Y, Xu X, Niu D, et al. Organophosphate flame retardants induce oxidative stress and Chop/Caspase 3-related apoptosis via Sod1/p53/Map3k6/Fkbp5 in NCI-1975 cells. Sci Total Environ. 2022;819:153160.
59. Kim C, Kim B. Anti-cancer natural products and their bioactive compounds inducing ER stress-mediated apoptosis: a review. Nutrients. 2018;10(8):1021.
60. Ghosh R, Wang L, Wang ES, et al. Allosteric inhibition of the IRE1α RNase preserves cell viability and function during endoplasmic reticulum stress. Cell. 2014;158(3):534–48.